



Blockade of Stat3 oncogene addiction induces cellular senescence and reveals a cell-nonautonomous activity suitable for cancer immunotherapy

Mara De Martino, Mercedes Tkach, Sofía Bruni, Darío Rocha, María F. Mercogliano, Mauro E. Cenciarini, María F. Chervo, Cecilia J. Proietti, Florent Dingli, Damarys Loew, Elmer A. Fernández, Patricia V. Elizalde, Eliane Piaggio & Roxana Schillaci

To cite this article: Mara De Martino, Mercedes Tkach, Sofía Bruni, Darío Rocha, María F. Mercogliano, Mauro E. Cenciarini, María F. Chervo, Cecilia J. Proietti, Florent Dingli, Damarys Loew, Elmer A. Fernández, Patricia V. Elizalde, Eliane Piaggio & Roxana Schillaci (2020) Blockade of Stat3 oncogene addiction induces cellular senescence and reveals a cell-nonautonomous activity suitable for cancer immunotherapy, *Oncolmmunology*, 9:1, 1715767, DOI: [10.1080/2162402X.2020.1715767](https://doi.org/10.1080/2162402X.2020.1715767)

To link to this article: <https://doi.org/10.1080/2162402X.2020.1715767>



© 2020 The Author(s). Published with license by Taylor & Francis Group, LLC.



[View supplementary material](#)



Published online: 29 Jan 2020.



[Submit your article to this journal](#)



Article views: 565






[View related articles](#)



[View Crossmark data](#)

Blockade of Stat3 oncogene addiction induces cellular senescence and reveals a cell-nonautonomous activity suitable for cancer immunotherapy

Mara De Martino ^{a*}, Mercedes Tkach ^b, Sofía Bruni ^a, Darío Rocha^c, María F. Mercogliano^a, Mauro E. Cenciarini^a, María F. Chervo^a, Cecilia J. Proietti ^a, Florent Dingli ^d, Damarys Loew ^d, Elmer A. Fernández^{c,e}, Patricia V. Elizalde ^a, Eliane Piaggio ^b, and Roxana Schillaci ^a

^aLaboratory of Molecular Mechanisms of Carcinogenesis, Instituto de Biología Y Medicina Experimental (IBYME-CONICET), Buenos Aires, Argentina; ^bInstitut Curie, PSL Research University, INSERM U932, Paris, France; ^cFacultad de Ciencias Exactas, Físicas Y Naturales, Universidad Nacional de Córdoba, Córdoba, Argentina; ^dInstitut Curie, PSL Research University, Centre de Recherche, Laboratoire de Spectrométrie de Masse Protéomique, Paris, France; ^eCentro de Investigación y Desarrollo en Inmunología y Enfermedades Infecciosas (CIDIE), Universidad Católica De Córdoba, Consejo Nacional de Investigaciones Científicas Y Técnicas (CONICET), Córdoba, Argentina

ABSTRACT

Stat3 is constitutively activated in several tumor types and plays an essential role in maintaining their malignant phenotype and immunosuppression. To take advantage of the promising antitumor activity of Stat3 targeting, it is vital to understand the mechanism by which Stat3 regulates both cell autonomous and non-autonomous processes. Here, we demonstrated that turning off Stat3 constitutive activation in different cancer cell types induces senescence, thus revealing their Stat3 addiction. Taking advantage of the senescence-associated secretory phenotype (SASP) induced by Stat3 silencing (SASP-siStat3), we designed an immunotherapy. The administration of SASP-siStat3 immunotherapy induced a strong inhibition of triple-negative breast cancer and melanoma growth associated with activation of CD4 + T and NK cells. Combining this immunotherapy with anti-PD-1 antibody resulted in survival improvement in mice bearing melanoma. The characterization of the SASP components revealed that type I IFN-related mediators, triggered by the activation of the cyclic GMP-AMP synthase DNA sensing pathway, are important for its immunosurveillance activity. Overall, our findings provided evidence that administration of SASP-siStat3 or low dose of Stat3-blocking agents would benefit patients with Stat3-addicted tumors to unleash an antitumor immune response and to improve the effectiveness of immune checkpoint inhibitors.

ARTICLE HISTORY

Received 1 November 2019
Revised 9 January 2020
Accepted 10 January 2020

KEYWORDS



Stat3; immunotherapy; senescence; oncogene addiction; immune checkpoint blockade

Introduction


Stat3 has been recognized as an oncogene as its activation promotes cellular transformation.¹ Stat3 constitutive activation contributes to cell survival, angiogenesis, and proliferation in a large variety of cancer types.^{2,3} In addition, Stat3 also controls innate and adaptive antitumor immune responses by the production of immunosuppressive factors that exert a “feed-forward” mechanism activating Stat3 in different immune cell subtypes.⁴ Indeed, it drives the differentiation of myeloid-derived suppressor cells (MDSCs) and regulatory T (Tregs) cells and hampers NK cell activation and CD8 + T cell cytotoxicity.^{5,6} Conversely, blockade of Stat3 activation in cancer cells induces an increase in pro-inflammatory mediators that leads to antitumor immunity.^{4,7} In line with these findings, we previously demonstrated that immunization with Stat3-blocked breast cancer cells induces an antitumor immune response involving CD4 + T and NK cells.⁸ However, the effect of Stat3 inhibition non-autonomous activity *in vivo* and the molecular mechanism that regulates the production of cytokines/chemokines able to reinstate immunosurveillance have not been addressed.

We have previously shown that Stat3 blockade in murine breast cancer models *in vitro*, induces cellular senescence.⁸ Cellular senescence is a stable cell growth arrest that can be induced by replicative exhaustion, chemotherapy or radiotherapy, or oncogenic stimuli, among others.⁹⁻¹² Another source of cellular senescence is related to oncogene addiction: cancer cells frequently become “addicted to” the constitutive activation or overexpression of a single oncogene to preserve their malignant phenotype.¹³ Blockade of oncogene addiction can reactivate cellular senescence, a process known as oncogene inhibition-induced senescence (OIIS).¹⁴ Senescent cells produce a secretory profile composed mainly of growth factors, cytokines, and proteinases, a signature termed senescence-associated secretory phenotype (SASP). The SASP can either foster tumorigenesis or stimulate the innate and adaptive antitumor immune response, a process called senescence immunosurveillance.^{15,16} Thus, we hypothesized that Stat3 blockade in cancer cells triggers an OIIS program able to secrete mediators that induce senescence immunosurveillance.

In this work, we report that targeting Stat3 in Stat3-addicted cancer cells turns them senescent and produces

CONTACT Roxana Schillaci  rschillaci@ibyme.conicet.gov.ar  Instituto de Biología Y Medicina Experimental (IBYME-CONICET), Vuelta de Obligado 2490, Buenos Aires, C1428ADN, Argentina

*Present address: Department of Radiation Oncology, Weill Cornell Medical College, New York, NY, USA.

 Supplemental data for this article can be accessed on the [publisher's website](#).

© 2020 The Author(s). Published with license by Taylor & Francis Group, LLC.

This is an Open Access article distributed under the terms of the Creative Commons Attribution-NonCommercial License (<http://creativecommons.org/licenses/by-nc/4.0/>), which permits unrestricted non-commercial use, distribution, and reproduction in any medium, provided the original work is properly cited.

a SASP able to unleash an antitumor immune response against established 4T1 murine triple-negative breast cancer and B16 melanoma. This SASP overcomes melanoma resistance to antiprogrammed cell death protein 1 (PD-1) antibody. We identify type I IFN-induced factors as the main components responsible for the immunosurveillance properties of the SASP and disclose the underlying mechanism of their production.

Materials and methods

Reagents and antibodies

Detailed information regarding the reagents and antibodies used in this study is provided in Supplem. Table 1.

Animals and tumors

Experiments were carried out with virgin female BALB/c mice, raised at the Institute of Biology and Experimental Medicine of Buenos Aires and with male C57BL/6 purchased from The Charles River Laboratories, and were maintained in pathogen-free conditions. All animal studies were conducted in accordance with the highest standards of animal care as outlined by the National Institutes of Health's Guide for the Care and Use of Laboratory Animals and were approved by the Institute of Biology and Experimental Medicine and Institute Curie Animal Research Committee. Progesterin-dependent ductal tumor line C4HD was originated in mice treated with 40 mg medroxyprogesterone acetate (MPA; Gador) every 3 months for 1 year and were maintained by serial transplantation in animals treated with 40 mg s.c. depot-MPA in the opposite flank to tumor inoculum.⁸

Cell lines and siRNA transfections

T-47D, BT-474, MDA-MB-468, MDA-MB-231, CT-26, HuVEC, YAC-1, and NCI-N87 cells were obtained from the American Type Culture Collection and JIMT-1 cells from the German Resource Center for Biological Material. KPL-4 and cells were kindly provided by Dr. J. Kurebayashi (Kawasaki Medical School, Kurashiki, Japan). B16F10-OVA (B16) melanoma cell line was kindly provided by Dr. K. Rock (University of Massachusetts Medical School, Boston, MA), and MCA101-OVA (MCA101) was kindly provided by Dr. Clothilde Théry (Institut Curie, PSL Research University INSERM U932, Paris, France). Primary cultures of epithelial cells from C4HD tumors growing in MPA treated mice were performed as described previously.⁸ Experiments and cell maintenance were performed in DMEM:F12 (1:1 v/v) or RPMI1640 medium (Life Technologies) supplemented with 10% heat-inactivated fetal bovine serum (FBS, Internegocios). Cells were routinely tested for Mycoplasma contamination.

siRNAs were synthesized by Dharmacon. Experiments were performed with at least two different siRNA sequences for each protein, but we here presented results obtained with only one of them. A control siRNA oligonucleotide from Dharmacon that does not target any known mammalian gene was used as a negative control. siRNAs were used at a final concentration of 100 nmol/L and were transfected with

Dharmafect1 reagent for 48 h according to the manufacturer's specifications and as we previously described.¹⁷

Conditioned medium

4T1, B16, MCA101, and MDA-MB-231 cells plated in 100-mm dishes were transiently transfected with the indicated siRNA or treated with 100 nmol/L doxorubicin (Abbot, Buenos Aires, Argentina). Then, cells were washed three times with PBS and cultured for 24 h with serum-free medium. After incubation, the conditioned medium (CM) was collected and centrifuged at 400 g. This CM was mixed with a complete medium in a proportion of 1 to 1 for *in vitro* studies. For *in vivo* administration, CM was collected, filtered through a 0.2- μ m pore filter, concentrated with spin-columns of 3kD cutoff (Merck Millipore) and lyophilized. The lyophilized CM was embedded in Elvax particles (DuPont)¹⁸ and implanted s.c. as a pellet to the animals.

Tumor experiments

Immunization protocol: BALB/c mice or C57BL/6 animals were injected s.c. with 1×10^4 4T1 or 1×10^5 B16 cells, respectively. When tumors reached 50 mm³, animals were immunized with 1×10^6 4T1 or B16 irradiated cells s.c. Simultaneously, a pellet of CM-siStat3 or CM-siControl was implanted s.c. This immunization was repeated three times according to the detailed experimental condition. In the indicated experiments, anti-PD-1 antibody (10 mg/kg) was administered i.p. Animals were monitored, and tumor width (W) and length (L) were measured with a Vernier caliper three times a week and tumor volume (mm³) was calculated as $(L \times W^2)/2$. Endpoint criteria for the survival studies included tumor volume exceeding 1000 mm³ or tumor ulceration.

Treatment with JSI-124: BALB/c or C57BL/6 animals was injected s.c. with 1×10^4 4T1 or 1×10^5 B16 cells, respectively. When tumors reached 100 mm³, animals were treated daily with 1 mg/kg JSI-124 i.p. Animals were monitored, and the tumor volume was measured three times a week.

Evaluation of pulmonary metastasis

BALB/c mice bearing 4T1 tumors were sacrificed, lungs were fixed in Bouin solution, and the number of superficial lung colonies was counted by an investigator who was blind to the experimental arm.

Preparation of cell suspensions

Subcutaneous tumors were collected and cut into small pieces and placed into 2.5 mL of CO₂ independent medium (Gibco, Thermo Fisher Scientific, Waltham, MA) containing 0.1 mg/mL DNase I and 0.1 mg/mL Liberase TL. After mechanical dissociation, samples were incubated with shaking at 37°C for 30 min. The cell suspension was then filtered with a 70- μ m cell strainer (BD Biosciences) for direct tumor cell analysis and further separated on a Percoll gradient (GE Healthcare Life Sciences) from 40% to 75% interface to recover mononuclear cells for immune cell infiltrate analysis.

Spleens were removed and dissected into small pieces and single-cell suspensions were obtained by mechanical disruption. A red blood cell lysis (5 min, room temperature) was performed using 1 ml ammonium–chloride–potassium lysis buffer.

Flow cytometry

Surface staining was performed at 4°C with the indicated antibodies resuspended in PBS with 2% FBS and 2 mM EDTA. All intracellular staining was performed using intracellular Fixation/Permeabilization buffer set (eBioscience/Thermo Fisher) according to the manufacturer's instructions. Live-cell detection was performed using the Zombie Aqua Fixable Viability Kit (Biolegend). Flow cytometry was performed on an LSR Fortessa or Canto II flow cytometer (BD Biosciences) and analyzed using FlowJo software (version 10x, BD Biosciences).

NK cell degranulation assay

For degranulation evaluation, splenocytes were cultured alone or with YAC-1 (1×10^4 cells) overnight at 37°C. During the last 4 h, CD107a antibody was added. Cells were harvested and stained with CD3 and CD49b antibodies to gate NK cells (CD3-CD49b+ cells) and to determine the percentage of CD107a+ cells by flow cytometry.

Detection of Ag-specific T cells by Enzyme-Linked ImmunoSpot Assay (ELISPOT)

IFN γ -producing antigen-specific CD8 T cells were measured by ELISPOT. Briefly, microplates (MAIP54510; Merck Millipore) were coated with antimurine IFN γ (Diacclone). Peripheral blood mononuclear cells (0.3×10^6) were cultured overnight in the presence of either control medium or class I-restricted OVA-I peptide (257–264, SIINFEKL, 10 mM). Cells and peptides were resuspended in complete medium RPMI supplemented with 10% FBS, 2 mM L-glutamine (Life Technologies), 1% penicillin/streptomycin (Life Technologies) and β -mercaptoethanol. Detection of IFN γ -producing cells was performed with biotinylated anti-IFN γ (matched pairs; Diaclone) followed by streptavidin–alkaline phosphatase (Mabtech) and revealed using the appropriate substrate (Bio-Rad). Spots were counted using an ELISPOT Reader System ELR02 (AID Diagnostika). Results were expressed as the number of cytokine-producing cells per 1×10^6 of total cells.

Cytokine production

For detecting cytokine and chemokine secretion, the CM-siStat3 and CM-siControl form 4T1 and B-16-OVA cells were evaluated using Proteome Profiler Mouse XL Cytokine Array developed according to the manufacturer's protocol (R&D Systems).

Evaluation of cytokine production (CXCL10, CCL2, CCL5, IL-15, IL-1 β , IL-6 and CXCL2) was quantified by sandwich

ELISA using paired cytokine-specific antibodies according to the manufacturer's instructions.

T cell activation and proliferation assays

Splenocytes were isolated from healthy BALB/c or C57BL/6 mice and T cells were purified by negative selection using EasySep™ (Stemcell Technologies) Mouse T Cell Isolation Kit according to the manufacturer's specifications. For activation and differentiation assay, T cells were stimulated with CD3/CD28 beads (Gibco, Thermo Fisher Scientific) for 72 h in 96-well plates using a 0.1:1 beads:lymphocyte ratio, and cells were stained with the indicated antibodies. For proliferation assay, stimulation with CD3/CD28 beads was performed for 72 h in 96-well plates using a 0.5:1 beads:lymphocyte ratio. In the last 6 h, a 0.5 μ Ci [3 H] thymidine (NEN, DuPont; specific activity: 20 Ci/mmol) was added. The assay was performed by quadruplicate as described previously.⁸ In some cases, antibodies anti-CCL2, CCL5, CXCR3, IL-15, and IFNAR were added at the beginning of the experiment.

C4HD, 4T1, MDA-MB-231, CT26, B16, MCA101, T-47D, and HuVEC cells were culture during 48 h, and a pulse of 0.5 μ Ci [3 H] thymidine was added in the last 16 h. In other set of experiments, tumor cells were transfected with siRNA Stat3 with or without siRNA p21^{CIP1} or p16^{INK4a} for 48 h.

Wound healing

A wound assay was employed to study the effect of CM-siStat3 of tumor cell on its cell migration. Wounds 400 μ m wide were made in confluent monolayers. Cells were treated with CM-siControl or CM-siStat3 obtained from the corresponding cell line and allowed to migrate into the cell-free area. At 18 h, cells were viewed and photographed with an inverted Olympus CKX41 microscope with 10 \times /0.25 objective using Olympus camera Q-Color 5. The cell-free wound area was quantified using ImageJ software (National Institutes of Health).

Sa- β -gal staining

Two methods were performed to assess the SA- β -gal activity at pH 6.0. Transfected cells grown on glass coverslips or frozen tumor tissues (10- μ m thickness) mounted on slides were washed in PBS, fixed in 3% formaldehyde, and washed again in PBS and incubated 16 h at 37°C without CO $_2$ with fresh SA- β -gal staining solution: 1 mg/mL 5-bromo-4-chloro-3-indolyl b-D-galactopyranoside (X-Gal) (Sigma Aldrich), 150 mM NaCl, 2 mM MgCl $_2$, 40 mM citric acid/Na phosphate buffer (pH 6), 5 mM potassium ferrocyanide, and 5 mM potassium ferricyanide. The stained cells and tissues were viewed and photographed with an inverted Olympus CKX41 microscope with 20X/0.4 objective using Olympus camera Q-Color 5. For the second method, we used 5-dodecanoylamino fluorescein di- β -d-galactopyranoside, obtained from Sigma-Aldrich as a substrate to detect SA- β -gal activity. Briefly, cells grown on 12-well plates were pretreated with 100 nmol/L bafilomycin A1 (Sigma-Aldrich) for 1 h at 37°C and 5% CO $_2$ humidified environment and then were

incubated with 33 $\mu\text{mol/L}$ C_{12}FDG for another 2 h. Cells were washed with PBS and analyzed by flow cytometry with the Canto II flow cytometer. The flow cytometry data were analyzed with FlowJo software.

Immunofluorescence detection of trimethyl K9 histone H3

Cells grown in glass coverslips were fixed and permeabilized with ice-cold methanol and were then blocked in PBS 1% bovine serum albumin (BSA). Trimethyl K9 histone H3 was detected using a rabbit mAb (Merck Millipore), followed by incubation with antirabbit IgG-Alexa 488 (Molecular Probes). Negative controls were carried out using PBS instead of primary antibodies. Nuclei were detected by propidium iodide (PI) staining (5 $\mu\text{g/ml}$). Cells were analyzed using a Nikon Eclipse E800 confocal laser microscopy system using a 60x/1.4 oil immersion objective. Quantitative analysis of confocal images was performed with ImageJ. We evaluated the integrated fluorescence intensity value for Trimethyl K9 histone H3 for 50 cells from each condition and obtained an average value. The nuclear compartment was defined according to the PI images. Fluorescence background (median) was subtracted in all cases.

Western blot analysis

Cells were lysed in a buffer containing 50mM Tris (pH 7.4), 150mM NaCl, 1mM EDTA, 1mM EGTA, 10% glycerol, 1% Nonidet P-40, 0.1% SDS, 1 mM Mg_2Cl , 1 mM phenylmethylsulfonylfluoride (PMSF), 10 $\mu\text{g/ml}$ leupeptin, 5 $\mu\text{g/ml}$ pepstatin, 5 $\mu\text{g/ml}$ aprotinin, 1 mM sodium orthovanadate and 25mM NaF. Lysates were centrifuged at 12,000 \times g for 30 min at 4°C and protein content in the supernatant was determined using a Bradford Proteins were solubilized in sample buffer (60 mM Tris-HCl, pH 6.8, 2% SDS, 10% glycerol, 0.7mM, 2 β mercaptoethanol, and 0.01% bromophenol blue) and subjected to SDS-PAGE. Proteins were electroblotted onto nitrocellulose. Membranes were immunoblotted with the antibodies shown in Supplem. Table 1. Enhanced chemiluminescence was performed according to the manufacturer's instructions (GE Healthcare). Signal intensities of phosphor-proteins were analyzed by densitometry using ImageJ software and normalized to total protein bands. Experiments assessing total protein content were also repeated three to five times and signal intensities were normalized to β -tubulin bands, used as loading control.

Proteomic studies

SILAC labeling, secretome collection 4T1 cells were cultured for 8 passages in SILAC media Arg- and Lys-free DMEM supplemented with "light" ($^{12}\text{C}_6$ $^{14}\text{N}_2$ -Lys and $^{12}\text{C}_6$ $^{14}\text{N}_4$ -Arg) or "heavy" ($^{12}\text{C}_6$ $^{15}\text{N}_2$ Lys and $^{12}\text{C}_6$ $^{15}\text{N}_4$ -Arg) isotopes. The stable isotope labeling was confirmed by LC-MS/MS after protein in-gel separation and digestion of blue bands.

4T1 cells labeled with "light" media were transfected with Control siRNA and cells labeled with "heavy" media were

transfected with Stat3 siRNA. After 48 h of transfection, cells were washed 5 times with PBS and cultured for another 24 h with serum-free medium.

For secretome collection, three secretomes of independent experiments were collected (total volume: 5 mL/condition), samples mixed in a 1:1 ratio and filtered through a 0.2 μm syringe filter. Samples were concentrated to 500 μl using centrifugal filtration units with 3 kD molecular weight cutoff.

Trypsin digestion Secretomes mixed at a 1:1 ratio were analyzed after a combination of FASP and fractionation through strong anion exchange separation. Ninety percent of each secretome was diluted in 500 μL of 25 mM ammonium bicarbonate before reduction with 5 mM dithiothreitol at 37°C for 1 h and alkylation with 10-mM iodoacetamide for 30 min at RT in the dark. Samples were then processed by a FASP procedure using 3kD Nanosep devices (Pall), according to standard protocols. Briefly, samples were loaded into the filtration devices and centrifuged at 13,000 g for 25 min. 500 μL of 25-mM ammonium bicarbonate was added and concentrated again. This step was repeated twice. The resulting concentrate was diluted to 200 μL with 25-mM ammonium bicarbonate and 2 μg trypsin/LysC was added. After overnight incubation at RT, peptides were collected by centrifugation of the filter units for 5 min. Strong anion exchange separation-based fractionation of peptides was performed as described.¹⁹ The six pH eluted fractions were loaded onto a homemade C18 SepPak-packed stage tip for desalting (principle by stacking one 3M Empore SPE Extraction Disk Octadecyl (C18) and beads from SepPak C18 Cartridge Waters into a 200- μL micropipette tip). Desalted samples were reconstituted in injection buffer (2% MeCN, 0.3% TFA) before LC-MS/MS analysis.

LC-MS/MS analysis Online LC was performed with an RSLCnano system (Ultimate 3000, Thermo Scientific) coupled online to an Orbitrap Fusion Tribrid mass spectrometer (MS, Thermo Scientific). Peptides were trapped on a C18 column (75- μm inner diameter \times 2 cm; nanoViper Acclaim PepMapTM 100, Thermo Scientific) with buffer A (2/98 MeCN/ H_2O in 0.1% formic acid) at a flow rate of 4.0 $\mu\text{L}/\text{min}$ over 4 min. Separation was performed on a 50 cm \times 75 μm C18 column (nanoViper Acclaim PepMapTM RSLC, 2 μm , 100 \AA , Thermo Scientific) regulated to a temperature of 55°C with a linear gradient of 5% to 25% buffer B (100% MeCN in 0.1% formic acid) at a flow rate of 300 nl/min over 100 min. Full-scan MS was acquired in the Orbitrap analyzer with a resolution set to 120,000, and ions from each full scan were HCD fragmented and analyzed in the linear ion trap.

Data Processing and Protein Identification Data were searched against the UniProtKB/Swiss-Prot Mus musculus database using SequestHT through Thermo Scientific Proteome Discoverer (v 2.1). The mass tolerances in MS and MS/MS were set to 10 ppm and 0.6 Da, respectively. We set carbamidomethyl cysteine, oxidation of methionine, N-terminal acetylation, heavy $^{13}\text{C}_6$ $^{15}\text{N}_2$ -Lysine (Lys8) and $^{13}\text{C}_6$ $^{15}\text{N}_4$ -Arginine (Arg10), medium $^2\text{H}_4$ -Lysine (Lys4), and $^{13}\text{C}_6$ -Arginine (Arg6) as variable modifications. We set specificity of trypsin digestion and allowed two missed cleavage sites.

The resulting files were further processed by using myProMS (v 3.5).²⁰ The Sequest HT target and decoy search result were validated at 1% false discovery rate with Percolator. For SILAC-based protein quantification, peptides XICs (Extracted Ion Chromatograms) were retrieved from Thermo Scientific Proteome Discoverer. Global MAD normalization was applied on the total signal to correct the XICs for each biological replicate (n = 3). Protein ratios were computed as the geometrical mean of related peptides. To estimate ratio significance, a t-test was performed with the R package limma²¹ and the false discovery rate has been controlled, thanks to the Benjamini-Hochberg procedure²² with a threshold set to 0.05. (All quantified proteins have at least two peptides quantified.) Data are available via ProteomeXchange with identifier PXD013948.²³ Secreted proteins were identified by Secretome P and Signal P databases using “The Human Cancer Secretome Database”²⁴ and MetaSecKB (<http://bioinformatics.yu.edu/secretomes/animal/index.php>).

TCGA data preparation

RNA-seq, Microarray and iTRAQ expression datasets for Breast Cancer were downloaded from TCGA²⁵ using TCGA-Assembler^{26,27} software pipeline. Only primary tumor samples were kept, for a total 1095 RNA-seq samples, 528 Microarray samples, and 105 iTRAQ samples. Out of those 105 iTRAQ samples, 28 were discarded (77 were kept) after a variance quality control.²⁸ Data were then normalized so that the expression had similar distributions across samples.

Samples were classified into breast-cancer intrinsic subtypes according to PAM50 molecular signature,²⁹ using PBCMC³⁰ R package with 10000 permutations, a 0.01 significance threshold, and a 0.1 correlation cutoff. To match TCGA data with the protein annotation obtained from myProMSoutput, MyGene.info³¹ annotation services were used.

Statistical analysis

All statistical analyses were performed using GraphPad Prism 6.0. The identity of the statistical test performed, *p* values and *n* values are stated in the figure legends. Longitudinal tumor growth data were analyzed using two-way ANOVA to assess overall group differences followed by Tukey post hoc comparisons. Comparison of the number of lung metastasis among different groups was done by the nonparametric Mann-Whitney U test. Survival was analyzed using the Kaplan-Meier model and log-rank Mantel-Cox test were used to compare two treatment groups. Differential expression analysis between breast cancer intrinsic subtypes in TCGA data was carried out using limma R package²¹ between basal-like and the other subtypes (Luminal A, Luminal B and Her2-enriched) and *p* values were adjusted using Benjamini-Hochberg procedure²² with a threshold set to 0.05. Parallelisms between CM-siStat3 treatment and breast cancer subtypes were studied through contingency tables and Pearson's chi-

squared test. A *p* value < 0.05 was accepted as statistically significant.

Results

Stat3 silencing induces senescence in Stat3-addicted cancer cells

To investigate the underlying cancer cell characteristics that dictate whether it can undergo senescence by Stat3 blockade, we silenced Stat3 by siRNA transfection in several cancer cell lines (Supplem. Figure 1(a)). Stat3 knockdown induced a sharp rise in senescence-associated β -galactosidase (SA- β -gal) activity and in heterochromatin formation trimethyl K9 histone H3, markers of cellular senescence,^{32,33} in HER2-positive breast cancer cells, triple-negative breast cancer, colon cancer, and melanoma (Figure 1(a) and Supplem. Figure 1(b,c)). However, no modulation of SA- β -gal was observed in fibrosarcoma MCA101 cells and in the luminal breast cancer BT-474 and T-47D cells (Figure 1(a) and Supplem. Figure 1(b)). Strikingly, all cell lines that experienced senescence after Stat3 knockdown had high levels of Stat3 phosphorylation at Tyr705. In contrast, senescence was absent in the cell lines in which Stat3 phosphorylation was barely detected (Figure 1(b)). Proliferation of C4HD, 4T1, MDA-MB-231, CT-26, and B16-OVA (hereafter abbreviated B16) cells was largely decreased after Stat3 silencing; meanwhile, MCA101 and T-47D cell proliferation was not affected (Figure 1(c)). Furthermore, senescence induced by Stat3 knockdown was dependent on the cyclin-dependent kinase inhibitors p16^{INK4} or p21^{CIP1} (Supplem. Figure 1(d-f)).³⁴

To study whether Stat3 inhibition-induced senescence also takes place *in vivo*, mice bearing 4T1 or B16 tumors were treated with the pharmacological inhibitor of Stat3 activation, JSI-124. Notably, the growth of both tumors was greatly suppressed by JSI-124 treatment (Figure 1(d)). The number of micrometastasis was decreased in mice bearing 4T1 tumor treated with the Stat3 inhibitor vs control counterpart (Supplem. Figure 2(a)). We observed strong SA- β -gal staining, and blockade of Stat3 phosphorylation in 4T1 and B16 tumors under JSI-124 treatment (Figure 1(e) and Supplem. Figure 2(b)). Altogether, our results demonstrate that Stat3 inhibition promotes a senescence program *in vitro* and *in vivo* in cancer cells that depend on Stat3 activation to maintain their malignant phenotype, thus revealing that they are Stat3-addicted. Therefore, Stat3 should be considered an oncogene whose inactivation leads to OIIS, as it has been demonstrated for *MYC*, *RAS*, and *BCR-ABL1*.^{35,36}

SASP from Stat3-silenced cells has anti-tumor and immune-stimulating activity in vitro

To evaluate the paracrine activity of the SASP induced by Stat3 silencing (SASP-siStat3) we used different cells of the tumor microenvironment to perform functional assays. To test this, we obtained the conditioned medium (CM) from 4T1, B16 and MDA-MB-231 cells transfected with Stat3 siRNA (CM-siStat3)

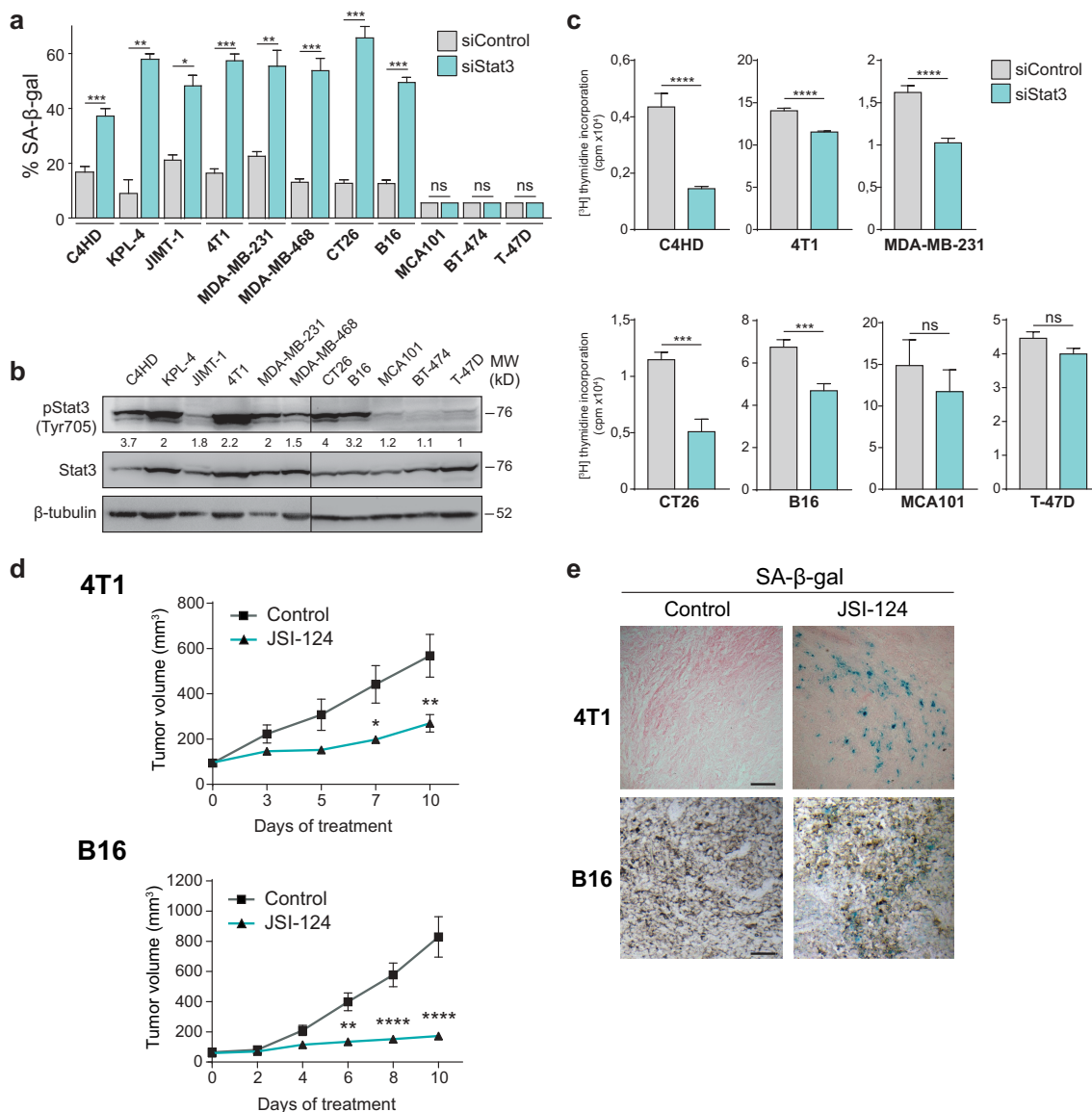


Figure 1. Stat3 silencing induces senescence in cancer cells addicted to Stat3 signaling pathway.

(a–c) Cells were transfected with 100 nmol/L control siRNA (siControl) or Stat3 siRNA (siStat3) for 48 h. (a) Senescence associated-β galactosidase (SA-β-gal) staining was performed and the graph shown the percentages of positive cells ($n = 50$, triplicates). (b) Immunoblot of phospho-Stat3 (pStat3 (Tyr705)) and Stat3 from cell lysates. Numbers below represent pStat3 (Tyr705)/Stat3 ratio. (c) Cell proliferation of transfected cells was determined by [^3H] thymidine incorporation at 48 h of culture. (d) BALB/c mice were injected s.c. with 10^4 4T1 cells and C57BL/6 mice were injected s.c. with 2×10^5 B16 cells. When tumors reached ~ 100 mm³ animals were injected i.p. with 1 mg/kg/day of JSI-124 ($n = 5$ –6 mice per group). Tumor volume was monitored along 10 days. (e) SA-β-gal staining was performed in tumors from vehicle- and JSI-124-treated animals. Representative photos are shown. Bars, 10 μm . Data are presented as means \pm SE. Data shown are representative of three independent experiments. p values were calculated using two-tailed Student's t test in **a**, **c** and two-way ANOVA test in **d**. ns, not significant, * $p < .05$, ** $p < .01$, *** $p < .001$, **** $p < .0001$.

or with control siRNA (CM-siControl). CM from MCA101 cells that did not undergo senescence upon Stat3 silencing (Figure 1(a)) was included as control. We observed that 4T1, B16, and MDA-MB-231 cells cultured with CM-siStat3 exhibited a decrease in proliferation and migration when compared to cells cultured with CM-siControl (Figure 2(a,b), respectively). When studying CM-siStat3 angiogenic potential, we revealed that CM-siStat3 from 4T1, B16, and MDA-MB-231 cells do not increase HUVEC proliferation vs. CM-siControl (Figure 2(c)). Finally, to investigate the immune-modulatory activities of the SASP-siStat3, we performed functional assays of murine T cells stimulated with anti-CD3/CD28-coated

beads. CM-siStat3 from 4T1 and B16 cells enhanced T cell proliferation in comparison with CM-siControl (Figure 2(d)). The CM-siStat3 from MCA101 cells showed similar behavior than CM-siControl in the above-mentioned assays (Figure 2(a–d)). As other control, we evaluated therapy-induced senescence by doxorubicin treatment (Supplement. Figure 3(a,b)). The CM from 4T1 and B16 cells treated with doxorubicin (CM-Doxorubicin) did not modify CD3/CD28-induced T cell proliferation vs control medium (Supplement. Figure 3(c)). Activation of CD4⁺ T cells, determined by CD69 expression, increased in the presence of CM-siStat3 vs CM-siControl from 4T1 and B16 cells (Figure 2(e)). In order to track the fate of naïve T cells

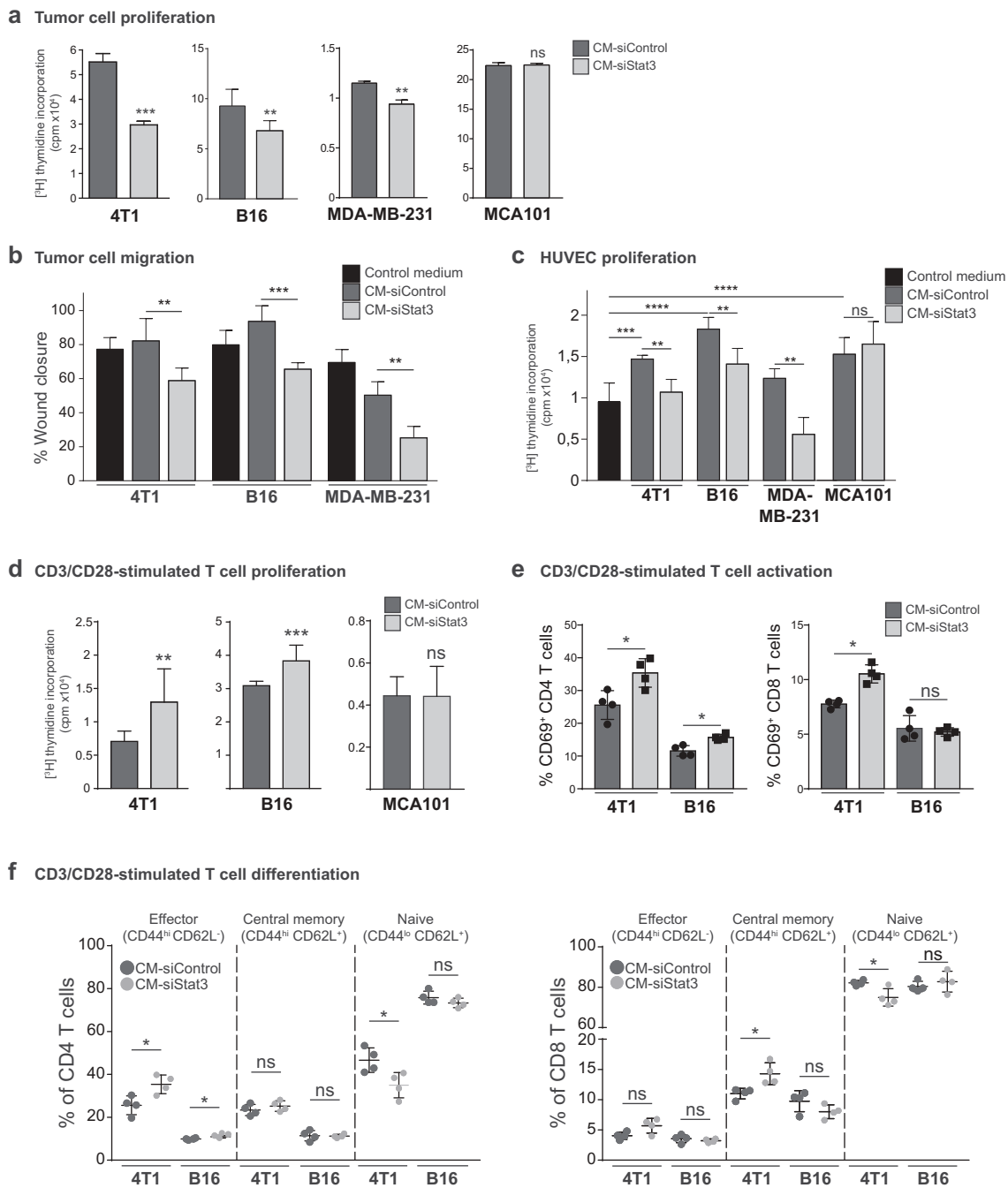


Figure 2. Antitumor activity of SASP from Stat3-silenced cancer cells.

4T1, B16, MDA-MB231, and MCA101 cells were transfected with 100 nmol/L siControl or siStat3 and conditioned mediums (CM-siControl or CM-siStat3, respectively) were obtained as described in Materials and methods. (a) Tumor cells were cultured for 48 h with CM-siControl or CM-siStat3 produced by the same cell line as indicated. Proliferation was determined by [³H] thymidine incorporation (n = 8). (b) Monolayers of tumor cells were wounded and allowed to migrate into the cell-free area in presence of CM-siControl or CM-siStat3 of tumor cells or control medium as indicated. Wounded areas were photographed at 0 and 18 h and quantified by densitometry (n = 4). (c) HUVEC cells were cultured for 48 h in presence of CM-siControl or CM-siStat3 of tumor cells or control medium as indicated, and proliferation was measured by [³H] thymidine incorporation (n = 8). (d-f) Purified T cells from spleen of BALB/c mice were activated with CD3/CD28 beads in the presence of CM-siControl or CM-siStat3 from 4T1 or MCA101 cells for 72 h. Similar protocols were followed with CM of B16 cells but T cells were isolated from the spleen of C57BL/6 mice. (d) Proliferation was determined by [³H] thymidine incorporation at 48 h (n = 8). (e) Activation of CD4⁺ or CD8⁺ T cells was determined immunofluorescence using anti-CD69 antibody and flow cytometry (n = 4). (f) Determination of CD4⁺ T and CD8⁺ T effector, central memory, and naïve T cells were determined by immunofluorescence using anti-CD62L and CD44 antibodies, and flow cytometry (n = 4). Data are presented as means ± SE. All data shown are representative of three independent experiments. *p* values were calculated using two-tailed Student's *t* test in **a, b, d-f** and by one-way ANOVA with Tukey's post-test in **c**. ns, not significant; **p* < .05, ***p* < .01, ****p* < .001, *****p* < .0001.

exposed to CM-siStat3, CD62L, and CD44 expression was determined. CM-siStat3 from 4T1 and B16 cells induced a significant increase of effector cells, a decrease of naïve cells

and no change in central memory CD4⁺ T cell subpopulation vs CM-siControl (Figure 2(f)). The CD8⁺ T cell subpopulation analysis revealed a significantly skew toward central memory

cells and away from naïve cells in CM-siStat3 vs CM-siControl only from 4T1 cells (Figure 2(f)). Collectively, these results indicate that the SASP-siStat3 has multiple paracrine antitumor effect, impairing tumor cell proliferation, migration, and angiogenic activity, while enhancing T cell proliferation and CD4 + T cell differentiation to an effector phenotype.

SASP-siStat3 is an adjuvant for a cellular cancer immunotherapy

The numerous *in vitro* antitumor effects of the SASP induced by Stat3 silencing described above encouraged us to study its application as a potential immunotherapy. Then, the CM-siStat3 and CM-siControl from 4T1 cells were concentrated, lyophilized, and embedded in Elvax particles.¹⁸ We designed a therapeutic administration protocol consisting of immunizations with wild type 4T1 irradiated tumor cells simultaneously with the administration of CM-siStat3 (SASP-siStat3 immunotherapy) or CM-siControl (Figure 3(a)). In animals treated with CM-siStat3, tumors grew strikingly more slowly and had fewer lung metastases than in the CM-siControl group (Figure 3(b,c)). CM-siStat3 immunized animals showed similar leukocyte and T-cell tumor infiltration to the CM-siControl group (Figure 3(d)), but CM-siStat3 immunized animals showed an increased percentage of effector CD4 + T cells (but not CD8 + T cells) in tumor and spleen (Figure 3(e)). NK cells from CM-siStat3 immunized animals also showed an increase in activation, measured by CD69 staining, both in tumor and spleen, compared to the CM-siControl group (Figure 3(f)). In regard to suppressor immune cells, CM-siStat3 immunized animals exhibited a significant decrease of Treg cell proportions in the tumor (but not in the spleen) (Figure 3(g)). The presence of monocytic MDSC (M-MDSC) was lower in the tumor of CM-siStat3 vs CM-siControl group, while for the granulocytic (MDSC) G-MDSC population, a trend was observed (Figure 3(h)). The antitumor effect of the SASP-siStat3 immunotherapy was dependent on the concomitant presence of an antigen source, provided by the irradiated cells, since the immunization with the CM-siStat3 alone did not impact tumor growth (data not shown).

To evaluate the clinical applicability of the treatment, we had analyzed the potential use of CM-siStat3 from cancer cells as an universal preparation suitable for treating different tumors. Thus, we injected 4T1 tumor-bearing mice with CM-siStat3 from a different cell type, the melanoma B16 cells, together with the irradiated 4T1 cells. Figure 3(j) shows that CM-siStat3 from B16 decreases 4T1 tumor growth with respect to animals treated with CM-siControl from B16. These results suggest the CM-siStat3 from cancer cells can have therapeutic potential.

We further evaluated the effectiveness of our immunotherapy protocol in the B16 preclinical model (Figure 4(a)). We observed a strong decrease of tumor growth in mice immunized with B16 irradiated cells and CM-siStat3 (Figure 4(b)) and an increase in the survival of these mice (Figure 4(c)), when compared to CM-siControl. To improve the efficacy of SASP-siStat3 immunotherapy, we used the checkpoint blocking antibody against PD-1 (Figure 4(a)). Notably, anti-PD1 antibody plus the CM-siStat3 combination showed a trend toward suppressed B16 tumor growth and synergistically improved mice survival with respect

to the CM-siStat3 alone (Figure 4(b,c)). In addition to the experiments testing tumor growth (Figure 4(b)), tumor regression was only observed in the combination group (2 out of 12 animals). It is noteworthy that anti-PD-1 monotherapy did not provide a measurable effect on survival or antitumor effect, nor did its combination with CM-siControl (Figure 4(b,c)). In addition, PD-L1 levels did not change in B16 cells cultured with CM-siStat3 with respect to CM-siControl (Supplem. Figure 4(a)). Similar results were found in 4T1 cells and tumors (Supplem. Figure 4(a,b)).

Administration of CM-siStat3 together with anti-PD1 antibody-induced antitumor specific CD8 + T cell response of about fivefold compared to CM-siStat3, measured by IFN- γ production (Figure 4(d)). The CM-Control+anti-PD-1 group tends to have more IFN- γ production than CM-Control group making it likely that anti-PD-1 might account for this effect. In addition, the combination therapy revealed an influx in the tumor microenvironment of leukocytes and T cells compared with the CM-siStat3 alone and control groups (Figure 4(e)). In accordance with the results obtained with 4T1 tumors, an increase in the proportion of effector CD4 + T cells in tumor and spleen was observed in the CM-siStat3 group, and this was in line with the results obtained *in vitro* (Figure 2(f)). NK cells were also more activated in the tumors and spleen of mice treated with CM-siStat3 vs. CM-siControl (Figure 4(g)). The addition of anti-PD-1 antibody to CM-siStat3 led to CD8 + T cell activation and differentiation to an effector phenotype in the tumor and spleen (Figure 4(f)). A decrease in Tregs infiltrating the tumor was also evident in CM-siStat3 (Figure 4(h)). Addition of anti-PD-1 antibody did not further decrease tumor-infiltrating Tregs. These data suggest that the SASP-siStat3 immunotherapy mobilized and activated CD4 + T and NK cells and acted in synergy with anti-PD-1 antibody, which, in turn, enhanced the expansion and activation of tumor-specific CD8 + T cells to obtain tumor clearance.

Then, we reasoned that combining a Stat3 inhibitor and PD-1 blockade could be another feasible antitumor strategy. Considering the toxicity of the Stat3 inhibitors in the clinical setting, we decided to administer JSI-124 every other day instead of every day (Figure 1(d)) together with anti-PD-1; the latter at the same dose as described in Figure 4b that showed to be ineffective to control B16 tumor growth. We observed that JSI-124 or anti-PD-1 alone has no antitumor effect. However, the combination of JSI-124 and anti-PD-1 was able to significantly inhibit B16 tumor growth (Figure 4(i)).

The SASP-siStat3 is enriched in chemokines and type I IFN-associated genes

To characterize the immunomodulatory composition of the SASP-siStat3, a multiplex membrane-based antibody array was used. We observed that 11 and 7 molecules were upregulated and 4 and 7 were downregulated in CM-siStat3 vs CM-siControl from 4T1 and B16 cells, respectively (Figure 5(a) and Supplem. Figure 5(a,b)). Among the downregulated cytokines, we detected vascular endothelial growth factor (VEGF), leukemia inhibitor factor (LIF) and regenerating islet-derived protein 3-gamma (Reg3G), all Stat3-regulated genes (Figure 5(a) and Supplem. Figure 5). In the repertoire of up-regulated

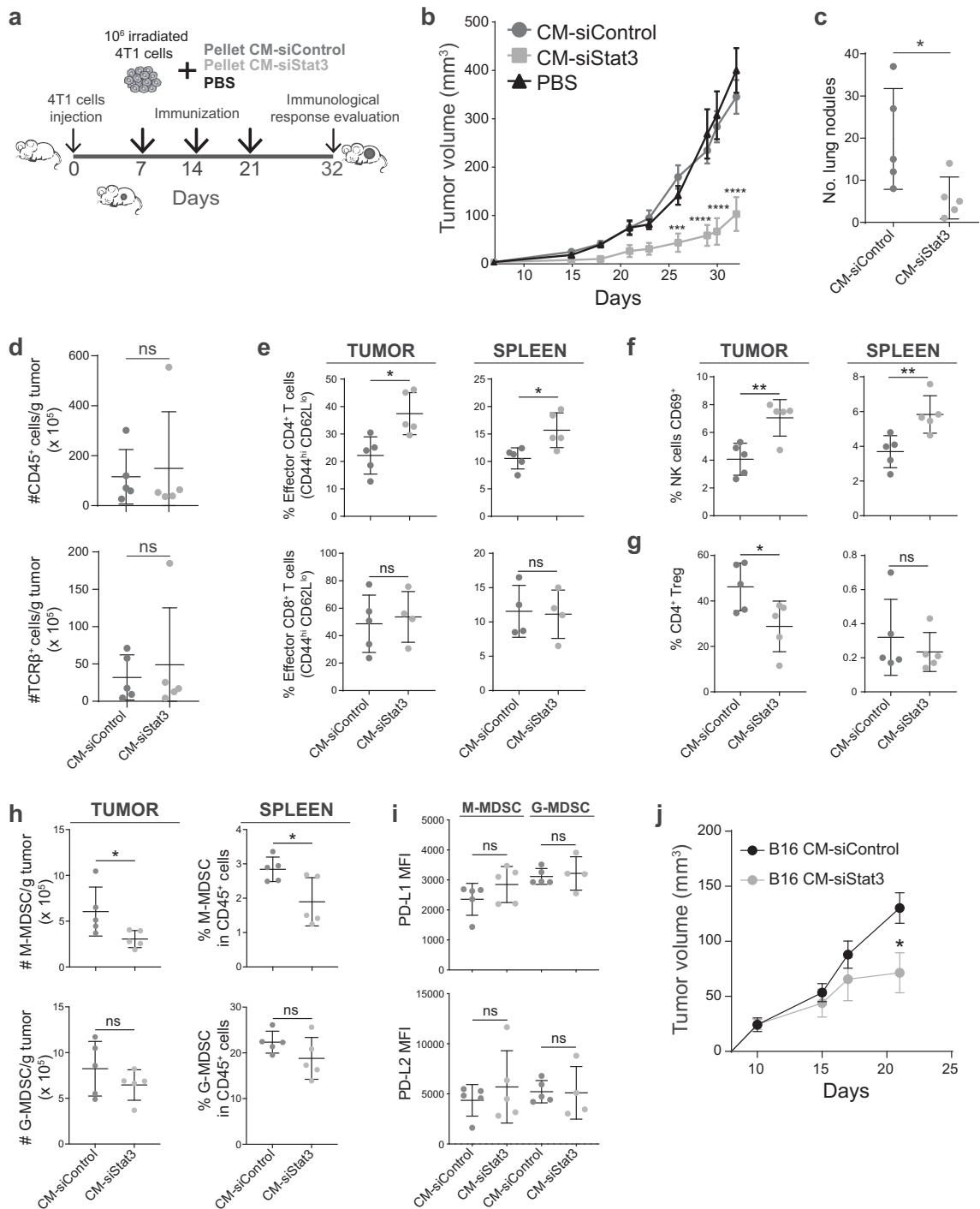


Figure 3. Immunotherapy of SASP from Stat3-silenced 4T1 cells with irradiated wild type cells promotes an antitumor immune response.

(a) Immunotherapy protocol. BALB/c mice were challenged s.c. with 10⁶ 4T1 cells. When tumors were palpable, animals were injected s.c. with 10⁶ irradiated 4T1 cells (100 Gy) and with a depot containing the lyophilized CM-siControl or CM-siStat3 from 4T1 cells once a week for 3 weeks. Control group received PBS and irradiated 4T1 cells. Ten days after the last immunization, mice were sacrificed and the immune response was evaluated (n = 5 mice per group). (b) Tumor volume was monitored along the experiment. (c) Lungs were harvested, fixed, and the number of 4T1 tumor nodules was counted. (d) Tumor-infiltrating leukocytes and T cells were determined by CD45 and TCRβ staining, respectively, and the number was referred to g tumor. (e) Effector CD4⁺ and CD8⁺ T cells were determined by CD44 and CD62L staining in tumor and spleen and analyzed by flow cytometry. (f) Intratumor and spleen NK cell activation was determined by staining with anti-CD69 on the CD3⁺/DX5⁺ population. (g) The percentage of Tregs (FOXP3⁺/CD25⁺) from total CD4⁺ T cells of the tumor and spleen was determined by immunofluorescence and analyzed by flow cytometry. (h) Tumor-infiltrating G-MDSC and M-MDSC populations were determined by Ly6C and Ly6G staining in the CD11b⁺ gate, and the number was referred to g tumor. In spleen, both populations were referred to as percentage of CD45⁺ cells. (i) PD-L1 and PD-L2 expression levels of G-MDSC and M-MDSC populations staining in tumor were analyzed by flow cytometry. (j) BALB/c mice were challenged s.c. with 10⁴ 4T1 cells. When tumors were palpable, animals were injected s.c. with 10⁶ irradiated 4T1 cells (100 Gy) and with a depot containing the lyophilized CM-siControl or CM-siStat3 from B16 cells once a week for 2 weeks. Tumor volume was monitored (n = 5 mice per group). Data are presented as means ± SE. Data shown are representative of three independent experiments **b-i** and of one experiment **j**. *p* values were calculated using two-way ANOVA test in **b, j** and two-tailed Student's *t* test in **c-i**. **p* < .05, ***p* < .01, ****p* < .001, *****p* < .0001.

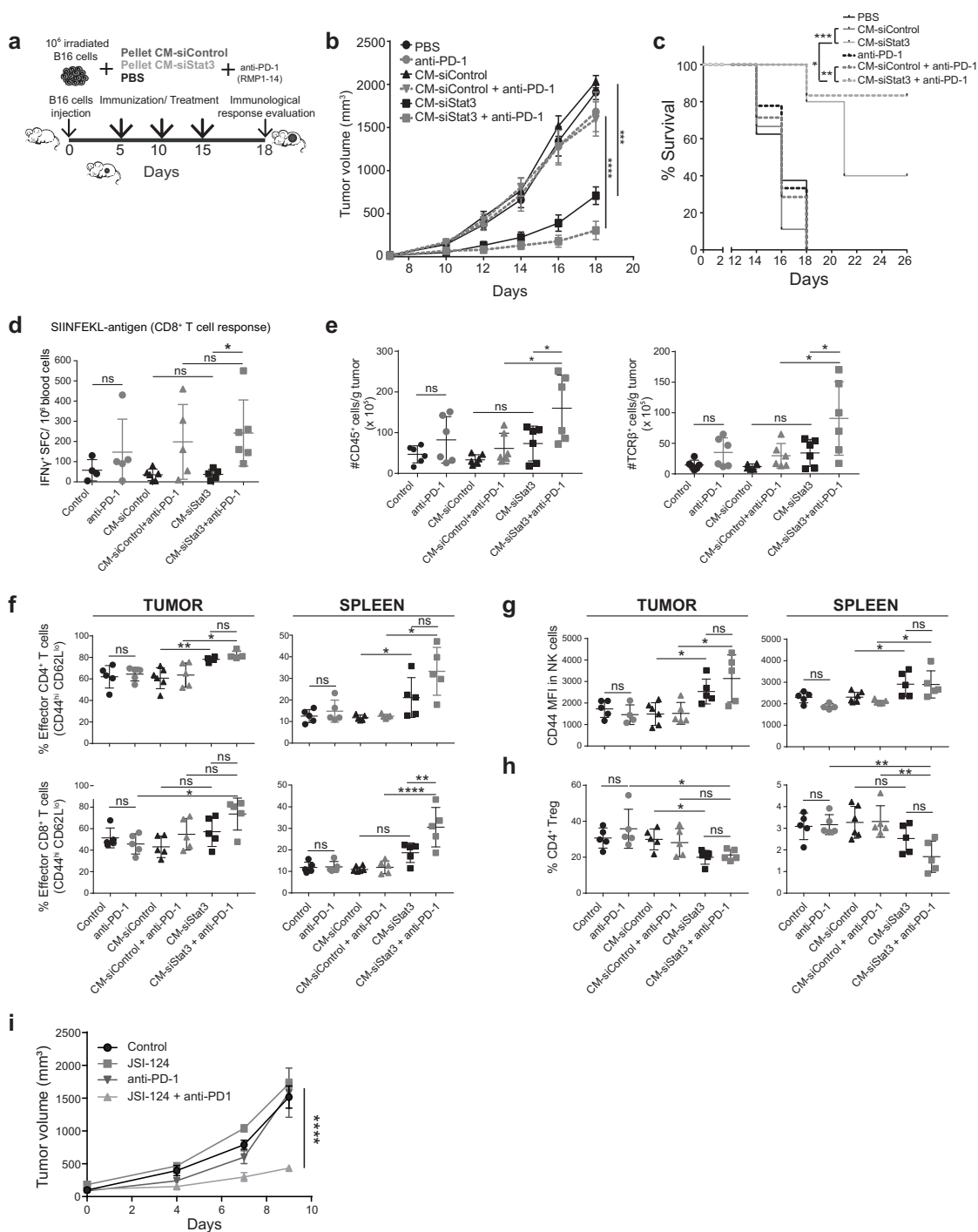


Figure 4. Immunotherapy with SASP from Stat3-silenced cancer cells acts in synergy with anti-PD-1 antibodies.

(a) Immunotherapy protocol. C57BL/6 mice were challenged s.c. with 2×10^5 B16 cells. When tumors were palpable, animals were injected s.c. with 10^6 irradiated B16 cells (100 Gy) and with a depot containing the lyophilized CM-siControl or CM-siStat3 from B16 cells every 5 days for 10 days. Three groups of animals received i.p. anti-PD-1 antibodies (10 mg/kg) at the same time of the above-mentioned immunotherapy. Control group received PBS and irradiated B16 cells. (b) Tumor volume was monitored along the experiment ($n = 6$ per group). (c) Survival curves exhibit differences of therapeutic efficacy of the immunotherapies in B16 melanoma. Percentage of survival represents either live mice or whose tumors were below 1000 mm³ ($n = 7-10$ mice per group). (d) IFN- γ production by OVA-specific CD8 + T cells determined by ELISPOT. Peripheral blood was obtained at day 14 and the production of IFN- γ was assessed by *ex-vivo* stimulation with SIINFEKL peptide. (e-h) Three days after the last immunization, mice were sacrificed and the immune response was evaluated. ($n = 6-5$ per group). (e) Tumor-infiltrating leukocytes and T cells were determined by CD45 and TCR β staining, respectively, and the number was referred to g tumor. (f) Effector CD4⁺ and CD8 + T cells were determined by CD44 and CD62L staining in tumor and spleen and analyzed by flow cytometry. (g) Spleen and tumor NK cell activation was determined by staining with anti-CD69 on the CD3⁻/NK1.1⁺ population and analyzed by flow cytometry. (h) Tregs from total CD4 + T-cells of the spleen and tumor were determined by immunofluorescence and analyzed by flow cytometry. (i) C57BL/6 mice were injected s.c. with 2×10^5 B16 cells. When tumors reached ~ 100 mm³ animals were injected i.p. with 1 mg/kg/day of JSI-124 ($n = 5$ mice per group) every other day, i.p. anti-PD-1 antibodies (10 mg/kg) on day 0 and 5 or both together. Control group was injected with rat IgG. Tumor volume was monitored for 9 days. Data are presented as means \pm SE. Data shown are representative of two independent experiments in **b**, **d-g**, cumulative of two independent experiments in **c** and of one experiment in **i**. *p* values were calculated using two-way ANOVA test in **b**, **i**, log-rank Mantel-Cox test comparing the two groups, in **c** and ANOVA with Tukey's posttest in **d-h**. ns, not significant, **p* < .05, ***p* < .01, ****p* < .001, *****p* < .0001.

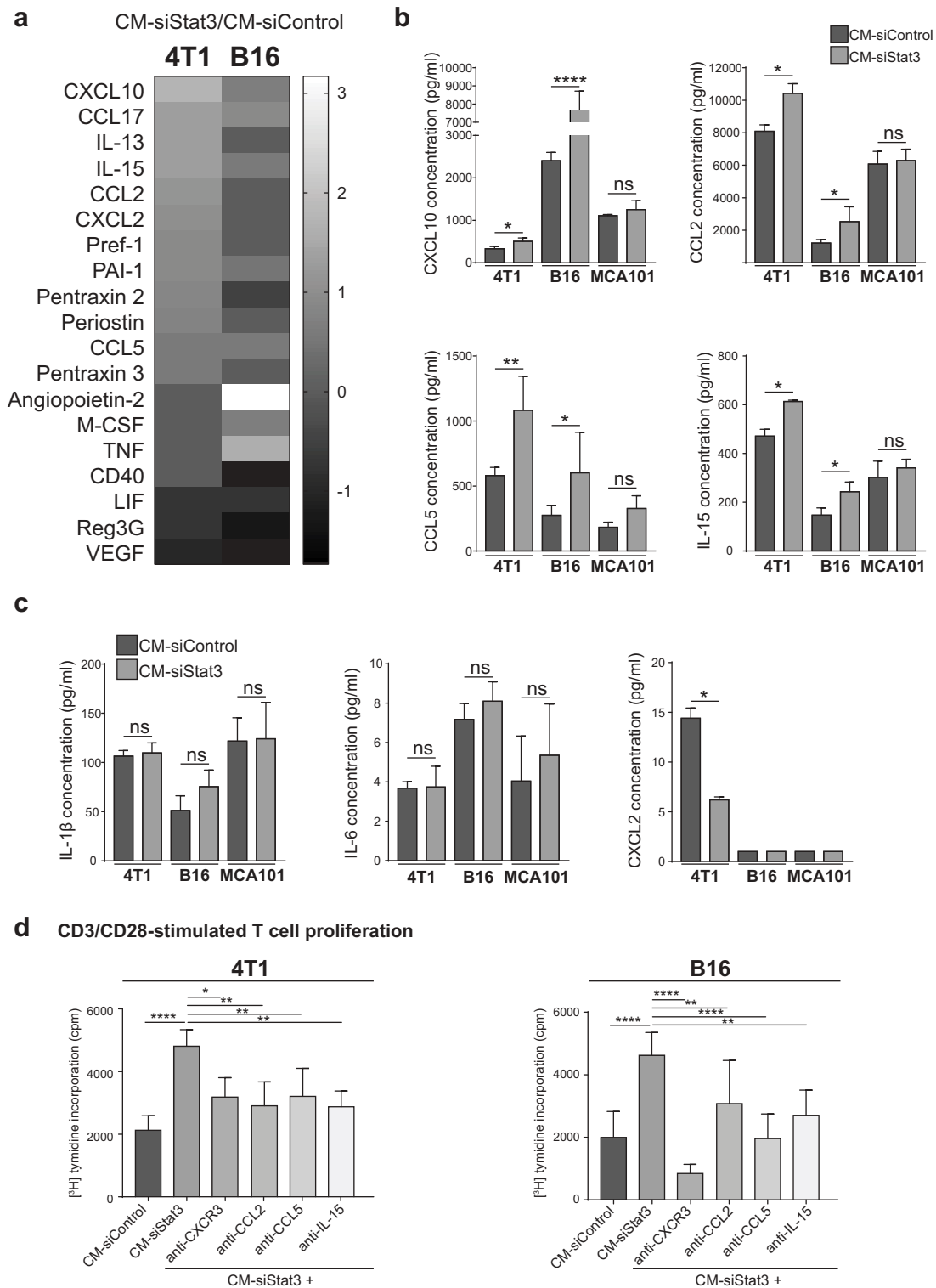


Figure 5. CCL2, CCL5, IL-15, and CXCL10 are mediators of the immune-stimulating activity of the SASP from Stat3-silenced cancer cells.

(a) CM-siControl and CM-siStat3 from 4T1 and B16 cells were analyzed using an antibody array for detecting cytokine and chemokine secretion. Heatmap of differentially expressed proteins in CM-siStat3 vs. CM-siControl. (b,c) Determination of different cytokines and chemokines in CM-siControl and CM-siStat3 from 4T1, B16, and MCA101 cells by ELISA. (d) Effect of neutralization of CXCR3, CCL2, CCL5, and IL-15 with specific antibodies on T cell proliferation. Purified T cells from spleen of BALB/c mice were activated with CD3/CD28 beads in the presence of CM-siControl or CM-siStat3 from 4T1 cells for 48 h and the corresponding Armenian hamster or goat control antibodies. In the case of CM-siStat3 different blocking antibodies were included. Data shown of CM-siControl and CM-siStat3 correspond to that obtained with Armenian hamster antibody, yielding similar results to those from goat antibody (not shown). Similar protocols were followed with CM from B16 cells but T cells were isolated from spleen of C57BL/6 mice. Proliferation was determined by ^3H thymidine incorporation at 72 h. Data are presented as means \pm SE. Data shown are representative of two (a, b), or three (c, d), independent experiments. *p* values were calculated using two-tailed Student's *t* test in b, c and by ANOVA with Tukey's posttest in d. ns, not significant, **p* < .05, ***p* < .01, ****p* < .001, *****p* < .0001.

factors in CM-siStat3 from 4T1 and B16 cells we observed an increase in IL-15 and the type I IFN-induced chemokines CXCL10/interferon inducible protein 10, C-C motif chemokine ligand 2 (CCL2) and CCL5 (Figure 5(a)), which are potent T cell- and NK cell-activating cytokine/chemokines.³⁷ These results were confirmed by ELISA, while these cytokine/chemokine levels in CM-siStat3 from MCA101 cells were similar to those obtained from CM-siControl (Figure 5(b)). The hallmark of SASPs induced by Ras activation, irradiation, or replicative senescence is the upregulation of IL-6, IL-1 β , and CXCL2/macrophage inflammatory protein 2, the mouse orthologous of human IL-8.³⁸ The ELISA determination of IL-1 β and IL-6 revealed that CM-siStat3 from 4T1, B16 and MCA101 cells had the same levels of these proinflammatory cytokines than CM-siControl (Figure 5(c)). CXCL2 levels were downregulated in CM-siStat3 in 4T1 cells, and undetectable in B16 and MCA101 cells. On the other hand, the CM-Doxorubicin exhibits an increase in CXCL10 in B16 cells and of CCL5 and CXCL2 in 4T1 cells (Supplem. Figure 3(d)). These data highlight the striking divergence of the SASP induced by Stat3 silencing in contrast with senescence induced by other types of insults.

To identify which cytokine/chemokine that emerged from the antibody array studies mediates the senescence immunosurveillance activity of the SASP-siStat3, we performed neutralization assays on T cells stimulated with anti-CD3/CD28-coated beads. Figure 5(d) shows that blockade of CCL2, CCL5, IL-15 and CXCR3 (CXCL10 receptor) reduced T cell proliferation exerted by CM-siStat3 from 4T1 and B16 cells compared to CM-siControl levels. These data suggest that multiple factors secreted by Stat3-silenced cells promote T cell proliferation.

We next sought to further decode the secreted proteins of SASP-siStat3 by quantitative proteomic profiling using stable isotope labeling of amino acids in cell culture (SILAC)-based proteomics on CM-siControl and CM-siStat3 from 4T1 cells (Supplem. Figure 6(a)). Among the 248 proteins found to be differentially regulated (greater than or equal to two-log fold change, $p < .05$) between CM-siStat3 and CM-siControl, 129 were upregulated and 119 were downregulated (Supplem. Figure 6(a) and Supplem. Table 2). The clustergram obtained using Wikipathway enrichment analysis on the upregulated and downregulated proteins identified processes involved in senescence and aging^{39,40} (Supplem. Figure 6(b)). Among the downregulated proteins we also found Stat3 and Stat3-regulated proteins such as CXCL1 (chemokine that recruits neutrophils and promotes angiogenesis) and CYR61 (growth and angiogenic factor) (Supplem. 6(b)), both proteins represented in the oncostatin/LIF signaling pathway.⁴¹

To further evaluate the clinical relevance of silencing Stat3, we studied whether the modulated proteins obtained from proteomic studies in CM-siControl compared to CM-siStat3 (CM-siStat3/CM-siControl) were also modulated in human basal-like subtype compared to other breast cancer subtypes. The comparison was centered in basal-like subtype because 60% of triple-negative breast carcinomas present that molecular profile. The analysis was carried out retrieving RNA-seq, Microarray and iTRAQ data from TCGA.²⁵ We observed a significant direct correlation between the up and

downregulated proteins in CM-siStat3/CM-siControl and their transcriptomic (RNA-seq and Microarray) and proteomic levels (iTRAQ) in luminal A/basal-like (Supplem. Figure 6(c)). Basal tumors stand out as aggressive and highly metastatic, while luminal A tumors stand out as more benign,²⁹ therefore the protein regulation observed in CM-siStat3 is concordant to a shift toward a more benign phenotype.

The induction of senescence and of type I IFN response induced by Stat3 silencing relies on cGAS

Most of the upregulated cytokines/chemokines found in the SASP that have an important role in T cell proliferation belong to the type I IFN response (Figure 5(d)). Indeed, proteomic data using Reactome showed that the term “immune system” was upregulated ($P = .004$) and IFN-induced protein 35 (IFI35) and IFN-stimulated gene 15 (ISG15) were represented.⁴² Recently, it was demonstrated that chromatin fragments in the cytosol of senescent cells trigger the cytosolic DNA sensor cGAS, which produces the second messenger cyclic-GMP-AMP that activates stimulator of interferon gene protein (STING), thus engaging the production of inflammatory cytokines, chemokines, and type I IFNs.^{43–47} Then, we studied the potential contribution of cGAS on senescence induced by Stat3 silencing and on immunosurveillance characteristic of its SASP. We observed that silencing cGAS did not affect senescence in 4T1 and B16 cells measured by 5-dodecanoylaminofluorescein di- β -D-galactopyranoside staining (Figure 6(a)). Blockade of cGAS expression completely inhibited senescence induced by Stat3 silencing. Remarkably, the production of type I IFN-related proteins, CXCL10, ISG15, and IFI35, produced by Stat3 depletion, was greatly compromised in the absence of cGAS (Figure 6(b,c)). Then, we observed that CM-siStat3+ sicGAS from 4T1 and B16 cells completely inhibited the CD3/CD28 T cell proliferation exerted by CM-siStat3 (Figure 6(d)) suggesting the involvement of type I IFN-related proteins in the stimulating activity in CM-siStat3. In addition, anti-IFN alpha receptor antibodies inhibited the ability of CM-siStat3 from 4T1 and B16 cells to enhance T cell proliferation (Figure 6(e)). To study the contribution of cGAS pathway on the antitumor immune response elicited by CM-siStat3, we went back to the immunization protocol using 4T1 tumor model but now including CM-siStat3+ sicGAS (Figure 6(f)). We observed that the simultaneous depletion of cGAS and Stat3 in 4T1 cells generates a CM that provides a partial protection from 4T1 tumor growth with respect to CM-siStat3 (Figure 6(g)). The CM-sicGAS exhibited no antitumor effect (Figure 6(g)). Together, these findings suggest that cGAS is a key player for senescence and for the expression of inflammatory mediators in Stat3-silenced senescent cells, thus implying its involvement in the generation of immunosurveillance upon targeting Stat3.

Discussion

Stat3 has long been recognized as an attractive target in oncology but, despite many efforts, chronic treatment of solid tumors with Stat3 inhibitory drugs in humans faced severe side effects. Therefore, to take advantage of the antitumor activity of Stat3 blockade, it is key to understand the

with the immunosurveillance properties of OIIS. Here, we prove that the SASP-siStat3 immunotherapy is able to inhibit breast cancer and melanoma growth and enhances the efficacy of anti-PD-1 antibody. In addition, we uncover that the cGAS DNA sensing pathway modulates the production of type I IFN-inducible genes triggered by Stat3 inhibition thus revealing a mechanism of the immunosurveillance properties of the SASP.

The SASP can have either pro or antitumor activities.^{15,48–51} Seminal works of Campisi's lab described that SASP from human fibroblast cell lines subjected to ionizing radiation, oxidative stress, oncogenic RAS expression, or loss of p53, had the ability to induce epithelial–mesenchymal transition and to stimulate invasion of tumor cells. In addition, chemotherapy-induced senescence can promote tumor clearance but the persistence of senescent cells can cause chronic inflammation, drug resistance, cancer relapse, and bone marrow suppression.^{52,53} Interestingly, tumor senescence induced by radiation, chemotherapy, and HER2 activation among others, has Stat3 activation as a hallmark, and Stat3-driven cytokines are the main mediators of the SASP with protumorigenic activity.^{51,54,55} In contrast, here we targeted Stat3 and observed a strong downregulation of LIF, CXCL2, Reg3G, and VEGF, thus obtaining a SASP with a completely different composition from that described under the above-mentioned insults. Toso and colleagues demonstrated that the SASP of *Pten*-deficient prostate tumors has a protumorigenic and chemoresistant activity due to constitutive activation of the Jak2/Stat3 pathway.⁵⁶ In line with our findings, they “reprogramed” this SASP phenotype by blocking Jak2, and observed tumor regression when docetaxel was simultaneously administered.⁵⁶ Based on these findings and our results, Stat3 inhibition could be an attractive strategy to reprogram the negative effects of the SASP induced by different insults. Our results highlight the potential translatability of the administration of CM-Stat3 from tumor cells in combination with radiotherapy, as well as low dose of Stat3 inhibitors together with anti-PD-1 strategies in the oncology arena. The observation that CM-siStat3 from B16 cells inhibits 4T1 tumor growth confirmed our previous data where we demonstrated that immunization with irradiated 4T1 cells transfected with a dominant negative plasmid of Stat3 (Stat3Y705F) inhibited CT-26 (colon cancer) and C4HD (ErbB-2+ breast cancer) tumor growth.⁸ These data suggest that a “universal” CM could be obtained or formulated from Stat3-addicted tumors. In particular, the application of clinical grade CM is an active field of research in the area of regenerative medicine. A phase I trial based on administration of CM from mesenchymal stromal stem cells in multiple sclerosis proved to be safe.⁵⁷

The SASP from OIIS has been poorly explored. Data available show upregulation of the antitumor factors IFN- γ , TNF α , eotaxin, IL-5, and CCL5 and downregulation of the protumoral factors IL-6 and VEGF, in Myc-inactivated T-cell acute lymphoblastic lymphoma grown in immunocompetent animals.⁴⁹ The secretion of the above-mentioned cytokines and chemokines relied on the presence of CD4 + T cells, and tumor clearance was dependent on NK cell activity.⁴⁹ In agreement with this report, we have previously demonstrated that immunization with irradiated Stat3-blocked tumor cells triggers an antitumor immune response dependent on CD4 + T and NK cells.⁸ Here, we re-

create a similar antitumor immune response by using the SASP-siStat3 immunotherapy. Neutralization of CXCR3, CCL2, CCL5, and IL-15 proves that all these cytokines/chemokines are required for the enhanced activity of the SASP on T cell proliferation. Recently, it has been described that the novel cytokine-like 1a (CYTL1) overexpression reduces spontaneous lung metastasis reducing Stat3 phosphorylation in 4T1 tumor and in the lung tissue.⁵⁸ These findings lead to another strategy feasible to block Stat3. Interestingly, proteomic studies of the SASP also reveal the upregulation of the type I IFN-regulated genes IFI35 and ISG15. It has already been described that Stat3 inhibition in cancer cells upregulates type I IFN improving immunosurveillance.^{4,59} In particular, Yang and colleagues reported that type I IFNs were involved in the antitumor effect of a combined therapy of Stat3 inhibitors and chemotherapy.⁵⁹

Additionally, senescent cells have aberrant cytosolic chromatin fragments that trigger innate DNA recognition and induce type I IFN production through the activation of the cGAS–STING pathway.^{43–47} Our current work refines this scenario by including cGAS as one of the principal mediators of OIIS, the production of cytokines and chemokines and the antitumor effect of the CM of cancer cells upon Stat3 silencing. The knowledge of the interaction of PD-1 with PD-L1 activates a critical immune checkpoint leading to T cell inhibition has been exploited by the therapeutic intervention of antibodies against PD-1 or PD-L1.^{60–62} However, the clinical effectiveness of these antibodies relies on the presence of a T cell-infiltrated tumor microenvironment.⁶³ Our results obtained in the melanoma model unveil a novel therapeutic strategy for tumors with poor immune cell infiltration, by combining SASP-siStat3 immunotherapy with anti-PD-1 antibodies. We demonstrate that the SASP-siStat3 contains chemokines able to recruit T cells and activate T and NK cells in the tumor bed, allowing the anti-PD-1 effect.

Our findings highlight that Stat3 addiction confers vulnerabilities to cancer cells and that targeting Stat3 triggers a senescence program that unleashes an antitumor immune response mediated by its SASP. This can open a potential clinical application of our findings, through stratification of tumors by Stat3 activation levels. Cancer patients with constitutive activation of Stat3 are candidates for a short-term treatment with Stat3-blocking strategies prior to or along with immune checkpoint inhibitors.

Acknowledgments

We thank A. Molinolo (UCSD, San Diego, CA) for his constant help and the mouse facility, mass spectrometry platform, and flow cytometry core from Institut Curie. We are grateful for V. Chiauzzi's technical assistance. G. González from Radiation Oncology SA, Buenos Aires, Argentina, is acknowledged for his expert support in cell irradiation. We are grateful to Fundación René Baron and Fundación Williams for their institutional support to IBYME-CONICET.

Disclosure of potential conflicts of interest

No potential conflicts of interest were disclosed.

Funding

This work was supported by grants from National Cancer Institute (Argentina) 2018, IDB/PICT 2017-1517 from the National Agency of Scientific Promotion of Argentina (ANPCyT), Florencio Fiorini Foundation and Alberto J. Roemmers Foundation awarded to RS; a grant from Oncomed-Reno, CONICET 1819/03, awarded to PVE and RS; grants from National Cancer Institute (Argentina) 2018, IDB/PICT 2015-1587, IDB/PICT 2017-1587, from ANPCyT, PID 2012-066 from Consejo Nacional de Investigaciones Científicas y Técnicas and from the National Institute of Cancer from Argentina (Argentina) 2018-2019, all of them awarded to PVE; IDB/PICT 2017-1770 grant from ANPCyT awarded to CJP, grants from “Région Ile-de-France” and Fondation pour la Recherche Médicale to DL, grants from Institute Curie, Institut National de la Santé et de la Recherche Médicale, Association pour la Recherche sur le Cancer (ARC PJA 20131200444); Labex DCBIOL (ANR-10-IDEX-0001-02 PSL and ANR-11-LABX0043), SIRIC INCa-DGOS-Inserm_12554 awarded to EP.

ORCID

Mara De Martino  <http://orcid.org/0000-0002-3049-6495>

Mercedes Tkach  <http://orcid.org/0000-0002-8011-9444>

Sofia Bruni  <http://orcid.org/0000-0001-7429-8039>

Cecilia J. Proietti  <http://orcid.org/0000-0001-5875-4540>

Florent Dingli  <http://orcid.org/0000-0002-7715-2446>

Damarys Loew  <http://orcid.org/0000-0002-9111-8842>

Patricia V. Elizalde  <http://orcid.org/0000-0002-5923-9898>

Eliane Piaggio  <http://orcid.org/0000-0002-2455-8442>

Roxana Schillaci  <http://orcid.org/0000-0002-7776-3378>

References

- Bromberg JF, Wrzeszczynska MH, Devgan G, Zhao Y, Pestell RG, Albanese C, Darnell JE Jr. Stat3 as an oncogene. *Cell*. 1999;98:295–303. doi:10.1016/S0092-8674(00)81959-5.
- Bowman T, Garcia R, Turkson J, Jove R. STATs in oncogenesis. *Oncogene*. 2000;19:2474–2488. doi:10.1038/sj.onc.1203527.
- Proietti CJ, Izzo F, Diaz Flaque MC, Cordo RR, Venturutti L, Mercogliano MF, De Martino M, Pineda V, Munoz S, Guzman P, et al. Heregulin co-opts PR transcriptional action via Stat3 role as a coregulator to drive cancer growth. *Mol Endocrinol*. 2015;29:1468–1485. doi:10.1210/me.2015-1170.
- Wang T, Niu G, Kortylewski M, Burdelya L, Shain K, Zhang S, Bhattacharya R, Gabrilovich D, Heller R, Coppola D, et al. Regulation of the innate and adaptive immune responses by Stat-3 signaling in tumor cells. *Nat Med*. 2004;10:48–54. doi:10.1038/nm976.
- Vasquez-Dunddel D, Pan F, Zeng Q, Gorbounov M, Albesiano E, Fu J, Blosser RL, Tam AJ, Bruno T, Zhang H, et al. STAT3 regulates arginase-I in myeloid-derived suppressor cells from cancer patients. *J Clin Invest*. 2013;123:1580–1589. doi:10.1172/JCI60083.
- Gotthardt D, Putz EM, Straka E, Kudweis P, Biaggio M, Poli V, Strobl B, Muller M, Sexl V. Loss of STAT3 in murine NK cells enhances NK cell-dependent tumor surveillance. *Blood*. 2014;124:2370–2379. doi:10.1182/blood-2014-03-564450.
- Yu H, Kortylewski M, Pardoll D. Crosstalk between cancer and immune cells: role of STAT3 in the tumour microenvironment. *Nat Rev Immunol*. 2007;7:41–51. doi:10.1038/nri1995.
- Tkach M, Coria L, Rosemblit C, Rivas MA, Proietti CJ, Diaz Flaque MC, Beguelin W, Frahm I, Charreau EH, Cassataro J, et al. Targeting Stat3 induces senescence in tumor cells and elicits prophylactic and therapeutic immune responses against breast cancer growth mediated by NK cells and CD4+ T cells. *J Immunol*. 2012;189:1162–1172. doi:10.4049/jimmunol.1102538.
- Johnson LM, Price DK, Figg WD. Treatment-induced secretion of WNT16B promotes tumor growth and acquired resistance to chemotherapy: implications for potential use of inhibitors in cancer treatment. *Cancer Biol Ther*. 2013;14:90–91. doi:10.4161/cbt.22636.
- Jones KR, Elmore LW, Jackson-Cook C, Demasters G, Povirk LF, Holt SE, Gewirtz DA. p53-Dependent accelerated senescence induced by ionizing radiation in breast tumour cells. *Int J Radiat Biol*. 2005;81:445–458. doi:10.1080/09553000500168549.
- Serrano M, Lin AW, McCurrach ME, Beach D, Lowe SW. Oncogenic ras provokes premature cell senescence associated with accumulation of p53 and p16INK4a. *Cell*. 1997;88:593–602. doi:10.1016/S0092-8674(00)81902-9.
- Hayflick L. The limited in vitro lifetime of human diploid cell strains. *Exp Cell Res*. 1965;37:614–636. doi:10.1016/0014-4827(65)90211-9.
- Weinstein IB. Cancer. Addiction to oncogenes—the achilles heel of cancer. *Science*. 2002;297:63–64. doi:10.1126/science.1073096.
- Felsher DW, Bishop JM. Reversible tumorigenesis by MYC in hematopoietic lineages. *Mol Cell*. 1999;4:199–207. doi:10.1016/S1097-2765(00)80367-6.
- Xue W, Zender L, Miething C, Dickins RA, Hernando E, Krizhanovsky V, Cordon-Cardo C, Lowe SW. Senescence and tumour clearance is triggered by p53 restoration in murine liver carcinomas. *Nature*. 2007;445:656–660. doi:10.1038/nature05529.
- Kang TW, Yevsa T, Woller N, Hoenicke L, Wuestefeld T, Dauch D, Hohmeyer A, Gereke M, Rudalska R, Potapova A, et al. Senescence surveillance of pre-malignant hepatocytes limits liver cancer development. *Nature*. 2011;479:547–551. doi:10.1038/nature10599.
- Mercogliano MF, De Martino M, Venturutti L, Rivas MA, Proietti CJ, Inurrigarro G, Frahm I, Allemand DH, Deza EG, Ares S, et al. TNFalpha-induced mucin 4 expression elicits trastuzumab resistance in HER2-positive breast cancer. *Clin Cancer Res*. 2017;23:636–648. doi:10.1158/1078-0432.CCR-16-0970.
- Kumamoto T, Huang EK, Paek HJ, Morita A, Matsue H, Valentini RF, Takashima A. Induction of tumor-specific protective immunity by in situ langerhans cell vaccine. *Nat Biotechnol*. 2002;20:64–69. doi:10.1038/nbt0102-64.
- Wisniewski JR, Zougman A, Nagaraj N, Mann M. Universal sample preparation method for proteome analysis. *Nat Methods*. 2009;6:359–362. doi:10.1038/nmeth.1322.
- Poulet P, Carpentier S, Barillot E. myProMS, a web server for management and validation of mass spectrometry-based proteomic data. *Proteomics*. 2007;7:2553–2556. doi:10.1002/pmic.200600784.
- Ritchie ME, Phipson B, Wu D, Hu Y, Law CW, Shi W, Smyth GK. limma powers differential expression analyses for RNA-sequencing and microarray studies. *Nucleic Acids Res*. 2015;43:e47. doi:10.1093/nar/gkv007.
- Benjamini Y, Drai D, Elmer G, Kafkafi N, Golani I. Controlling the false discovery rate in behavior genetics research. *Behav Brain Res*. 2001;125:279–284. doi:10.1016/S0166-4328(01)00297-2.
- Vizcaino JA, Csordas A, Del Toro N, Dianes JA, Griss J, Lavidas I, Mayer G, Perez-Riverol Y, Reisinger F, Ternent T, et al. update of the PRIDE database and its related tools. *Nucleic Acids Res*. 2016;44:11033. doi:10.1093/nar/gkv1145.
- Feizi A, Banaei-Esfahani A, Nielsen J. HCSD: the human cancer secretome database. *Database*. 2015. doi:10.1093/database/bav051.
- Weinstein JN, Collisson EA, Mills GB, Shaw KR, Ozenberger BA, Ellrott K, Shmulevich I, Sander C, Stuart JM. The cancer genome atlas pan-cancer analysis project. *Nat Genet*. 2013;45:1113–1120. doi:10.1038/ng.2764.
- Wei L, Jin Z, Yang S, Xu Y, Y Z, Ji Y. TCGA-assembler 2: software pipeline for retrieval and processing of TCGA/CPTAC data. *Bioinformatics*. 2018;34:1615–1617. doi:10.1093/bioinformatics/btx812.
- R: A Language and Environment for Statistical Computing. R Core Team organization = R Foundation for Statistical Computing. Vienna, Austria; 2018. <https://www.R-project.org/>
- Mertins P, Mani DR, Ruggles KV, Gillette MA, Clauser KR, Wang P, Wang X, Qiao JW, Cao S, Petralia F, et al. Proteogenomics connects somatic mutations to signalling in breast cancer. *Nature*. 2016;534:55–62. doi:10.1038/nature18003.
- Parker JS, Mullins M, Cheang MC, Leung S, Voduc D, Vickery T, Davies S, Fauron C, He X, Hu Z, et al. Supervised risk predictor of breast cancer based on intrinsic subtypes. *J Clin Oncol*. 2009;27:1160–1167. doi:10.1200/JCO.2008.18.1370.

30. Fresno C, Gonzalez GA, Merino GA, Flesia AG, Podhjaer OL, Llera AS, Fernández E. A novel non-parametric method for uncertainty evaluation of correlation-based molecular signatures: its application on PAM50 algorithm. *Bioinformatics*. 2017;33:693–700. doi:10.1093/bioinformatics/btw704.
31. Xin J, Mark A, Afrasiabi C, Tsueng G, Juchler M, Gopal N, Stupp GS, Putman TE, Ainscough BJ, Griffith OL, et al. High-performance web services for querying gene and variant annotation. *Genome Biol*. 2016;17(1):1–7. doi:10.1186/s13059-016-0953-9.
32. Dimri GP, Lee X, Basile G, Acosta M, Scott G, Roskelley C, Medrano EE, Linskens M, Rubelj I, Pereira-Smith O, et al. A biomarker that identifies senescent human cells in culture and in aging skin in vivo. *Proc Natl Acad Sci U S A*. 1995;92:9363–9367. doi:10.1073/pnas.92.20.9363.
33. Narita M, Nunez S, Heard E, Narita M, Lin AW, Hearn SA, Spector DL, Hannon GJ, Lowe SW. Rb-mediated heterochromatin formation and silencing of E2F target genes during cellular senescence. *Cell*. 2003;113:703–716. doi:10.1016/S0092-8674(03)00401-X.
34. Krishnamurthy J, Torrice C, Ramsey MR, Kovalev GI, Al Regaiey K, Su L, Sharpless NE. Ink4a/Arf expression is a biomarker of aging. *J Clin Invest*. 2004;114:1299–1307. doi:10.1172/JCI22475.
35. Jain M, Arvanitis C, Chu K, Dewey W, Leonhardt E, Trinh M, Sundberg CD, Bishop JM, Felsner DW. Sustained loss of a neoplastic phenotype by brief inactivation of MYC. *Science*. 2002;297:102–104. doi:10.1126/science.1071489.
36. Tharkar-Promod S, Johnson DP, Bennett SE, Dennis EM, Banowsky BG, Jones SS, Shearstone JR, Quayle SN, Min C, Jarpe M, et al. HDAC1,2 inhibition and doxorubicin impair Mre11-dependent DNA repair and DISC to override BCR-ABL1-driven DSB repair in Philadelphia chromosome-positive B-cell precursor acute lymphoblastic leukemia. *Leukemia*. 2018;32:49–60. doi:10.1038/leu.2017.174.
37. Rauch I, Muller M, Decker T. The regulation of inflammation by interferons and their STATs. *JAKSTAT*. 2013;2:e23820. doi:10.4161/jkst.23820.
38. Freund A, Orjalo AV, Desprez PY, Campisi J. Inflammatory networks during cellular senescence: causes and consequences. *Trends Mol Med*. 2010;16:238–246. doi:10.1016/j.molmed.2010.03.003.
39. Hernandez-Segura A, de Jong TV, Melov S, Gurjev V, Campisi J, Demaria M. Unmasking transcriptional heterogeneity in senescent cells. *Curr Biol*. 2017;27:2652–2660. doi:10.1016/j.cub.2017.07.033.
40. Uthus EO, Brown-Borg HM. Altered methionine metabolism in long living Ames dwarf mice. *Exp Gerontol*. 2003;38:491–498. doi:10.1016/S0531-5565(03)00008-1.
41. Chen Y, Du XY. Functional properties and intracellular signaling of CCN1/Cyr61. *J Cell Biochem*. 2007;100:1337–1345. doi:10.1002/jcb.21194.
42. de Veer MJ, Holko M, Frevel M, Walker E, Der S, Paranjape JM, Silverman RH, Williams BR. Functional classification of interferon-stimulated genes identified using microarrays. *J Leukoc Biol*. 2001;69:912–920. doi:10.1189/jlb.69.6.912.
43. Yang H, Wang H, Ren J, Chen Q, Chen ZJ. cGAS is essential for cellular senescence. *Proc Natl Acad Sci U S A*. 2017;114:E4612–E4620. doi:10.1073/pnas.1705499114.
44. Dou Z, Ghosh K, Vizioli MG, Zhu J, Sen P, Wangenstein KJ, Simithy J, Lan Y, Lin Y, Zhou Z, et al. Cytoplasmic chromatin triggers inflammation in senescence and cancer. *Nature*. 2017;550:402–406. doi:10.1038/nature24050.
45. Gluck S, Guey B, Gulen MF, Wolter K, Kang TW, Schmacke NA, Bridgeman A, Rehwinkel J, Zender L, Ablasser A. Innate immune sensing of cytosolic chromatin fragments through cGAS promotes senescence. *Nat Cell Biol*. 2017;19:1061–1070. doi:10.1038/ncb3586.
46. Galluzzi L, Vanpouille-Box C, Bakhomou SF, Demaria S. Snapshot: CGAS-STING Signaling. *Cell*. 2018;173:276. doi:10.1016/j.cell.2018.03.015.
47. Vanpouille-Box C, Demaria S, Formenti SC, Galluzzi L. Cytosolic DNA sensing in organismal tumor control. *Cancer Cell*. 2018;34:361–378. doi:10.1016/j.ccell.2018.05.013.
48. Coppe JP, Patil CK, Rodier F, Sun Y, Munoz DP, Goldstein J, Nelson PS, Desprez PY, Campisi J. Senescence-associated secretory phenotypes reveal cell-nonautonomous functions of oncogenic RAS and the p53 tumor suppressor. *PLoS Biol*. 2008;6:2853–2868. doi:10.1371/journal.pbio.0060301.
49. Rakhra K, Bachireddy P, Zabuawala T, Zeiser R, Xu L, Kopelman A, Fan AC, Yang Q, Braunstein L, Crosby E, et al. CD4(+) T cells contribute to the remodeling of the microenvironment required for sustained tumor regression upon oncogene inactivation. *Cancer Cell*. 2010;18:485–498. doi:10.1016/j.ccr.2010.10.002.
50. Liu D, Hornsby PJ. Senescent human fibroblasts increase the early growth of xenograft tumors via matrix metalloproteinase secretion. *Cancer Res*. 2007;67:3117–3126. doi:10.1158/0008-5472.CAN-06-3452.
51. Zacarias-Fluck MF, Morancho B, Vicario R, Luque GA, Escorihuela M, Villanueva J, Rubio IT, Arribas J. Effect of cellular senescence on the growth of HER2-positive breast cancers. *J Natl Cancer Inst*. 2015;107. doi:10.1093/jnci/djv020.
52. Ewald JA, Desotelle JA, Wilding G, DF J. Therapy-induced senescence in cancer. *J Natl Cancer Inst*. 2010;102:1536–1546. doi:10.1093/jnci/djq364.
53. Demaria M, O’Leary MN, Chang J, Shao L, Liu S, Alimirah F, Koenig K, Le C, Mitin N, Deal AM, et al. Cellular senescence promotes adverse effects of chemotherapy and cancer relapse. *Cancer Discov*. 2017;7:165–176. doi:10.1158/2159-8290.CD-16-0241.
54. Ohanna M, Cheli Y, Bonet C, Bonazzi VF, Allegra M, Giuliano S, Bille K, Bahadoran P, Giaccherio D, Lacour JP, et al. Secretome from senescent melanoma engages the STAT3 pathway to favor reprogramming of naive melanoma towards a tumor-initiating cell phenotype. *Oncotarget*. 2013;4:2212–2224. doi:10.18632/oncotarget.1143.
55. Yu YC, Yang PM, Chuah QY, Huang YH, Peng CW, Lee YJ, Chiu SJ. Radiation-induced senescence in securin-deficient cancer cells promotes cell invasion involving the IL-6/STAT3 and PDGF-BB/PDGFR pathways. *Sci Rep*. 2013;3:1675. doi:10.1038/srep01675.
56. Toso A, Revandkar A, Di Mitri D, Guccini I, Proietti M, Sarti M, Pinton S, Zhang J, Kalathur M, Civenni G, et al. Enhancing chemotherapy efficacy in Pten-deficient prostate tumors by activating the senescence-associated antitumor immunity. *Cell Rep*. 2014;9:75–89. doi:10.1016/j.celrep.2014.08.044.
57. Dahbour S, Jamali F, Alhattab D, Al Radaideh A, Ababneh O, Al Ryalat N, Al Bdour M, Hourani B, Msallam M, Rasheed M, et al. Mesenchymal stem cells and conditioned media in the treatment of multiple sclerosis patients: clinical, ophthalmological and radiological assessments of safety and efficacy. *CNS Neurosci Ther*. 2017;23:866–874. doi:10.1111/cns.12759.
58. Wang X, Li T, Cheng Y, Wang P, Yuan W, Liu Q, Yang F, Liu Q, Ma D, Ding S, et al. CYTL1 inhibits tumor metastasis with decreasing STAT3 phosphorylation. *Oncoimmunology*. 2019;8:e1577126. doi:10.1080/2162402X.2019.1577126.
59. Yang H, Yamazaki T, Pietrocola F, Zhou H, Zitvogel L, Ma Y, Kroemer G. STAT3 inhibition enhances the therapeutic efficacy of immunogenic chemotherapy by stimulating type I interferon production by cancer cells. *Cancer Res*. 2015;75:3812–3822. doi:10.1158/0008-5472.CAN-15-1122.
60. Freeman GJ, Long AJ, Iwai Y, Bourque K, Chernova T, Nishimura H, Fitz LJ, Malenkovich N, Okazaki T, Byrne MC, et al. Engagement of the PD-1 immunoinhibitory receptor by a novel B7 family member leads to negative regulation of lymphocyte activation. *J Exp Med*. 2000;192:1027–1034. doi:10.1084/jem.192.7.1027.
61. Wang C, Thudium KB, Han M, Wang XT, Huang H, Feingersh D, Garcia C, Wu Y, Kuhne M, Srinivasan M, et al. In vitro characterization of the anti-PD-1 antibody nivolumab, BMS-936558, and in vivo toxicology in non-human primates. *Cancer Immunol Res*. 2014;2:846–856. doi:10.1158/2326-6066.CIR-14-0040.
62. Sharma P, Allison JP. The future of immune checkpoint therapy. *Science*. 2015;348:56–61. doi:10.1126/science.aaa8172.
63. Ji RR, Chasalow SD, Wang L, Hamid O, Schmidt H, Cogswell J, Alaparthi S, Berman D, Jure-Kunkel M, Siemers NO, et al. An immune-active tumor microenvironment favors clinical response to ipilimumab. *Cancer Immunol Immunother*. 2012;61:1019–1031. doi:10.1007/s00262-011-1172-6.